RESEARCH ARTICLE

Development of Cortical Morphology Evaluated with Longitudinal MR Brain Images of Preterm Infants

Pim Moeskops[1,2]*, Manon J. N. L. Benders[2,3,4], Karina J. Kersbergen[2], Floris Groenendaal[2,4], Linda S. de Vries[2,4], Max A. Viergever[1], Ivana Išgum[1,4]

1 Image Sciences Institute, University Medical Center Utrecht, Utrecht, The Netherlands, 2 Department of Neonatology, University Medical Center Utrecht, Utrecht, The Netherlands, 3 Department of Perinatal Imaging & Health, Division of Imaging Sciences & Biomedical Engineering, King's College London, London, United Kingdom, 4 Brain Center Rudolf Magnus, University Medical Center Utrecht, Utrecht, The Netherlands

* p.moeskops@umcutrecht.nl

Abstract

Introduction

The cerebral cortex develops rapidly in the last trimester of pregnancy. In preterm infants, brain development is very vulnerable because of their often complicated extra-uterine conditions. The aim of this study was to quantitatively describe cortical development in a cohort of 85 preterm infants with and without brain injury imaged at 30 and 40 weeks postmenstrual age (PMA).

Methods

In the acquired T_2-weighted MR images, unmyelinated white matter (UWM), cortical grey matter (CoGM), and cerebrospinal fluid in the extracerebral space (CSF) were automatically segmented. Based on these segmentations, cortical descriptors evaluating volume, surface area, thickness, gyrification index, and global mean curvature were computed at both time points, for the whole brain, as well as for the frontal, temporal, parietal, and occipital lobes separately. Additionally, visual scoring of brain abnormality was performed using a conventional scoring system at 40 weeks PMA.

Results

The evaluated descriptors showed larger change in the occipital lobes than in the other lobes. Moreover, the cortical descriptors showed an association with the abnormality scores: gyrification index and global mean curvature decreased, whereas, interestingly, median cortical thickness increased with increasing abnormality score. This was more pronounced at 40 weeks PMA than at 30 weeks PMA, suggesting that the period between 30 and 40 weeks PMA might provide a window of opportunity for intervention to prevent delay in cortical development.

Introduction

During the third trimester of pregnancy, the cerebral cortex develops from a smooth surface to a folded structure with high complexity, resembling the morphology of the adult cortex [1]. In preterm infants, neurodevelopment is particularly vulnerable due to extra-uterine complications, leading to primary brain injury and secondary developmental consequences [2–4].

In this population, it has been described that the development of the cerebral cortex, with respect to changes in surface area [5,6] and cortical folding [7], might be related to functional and cognitive development. Furthermore, preterm infants exhibit abnormal development of cortical thickness when measured in adolescence [8–10]. In normal development, thinning of the cerebral cortex by pruning of dispensable neurons and synapses, leading to more efficient synaptic connections, occurs during childhood and adolescence [11–14] and continues with aging [15,16]. In preterm infants, this process seems to be disturbed [10]. Some studies found that preterm infants have larger cortical grey matter (CoGM) volumes compared to healthy infants in several regions at term equivalent age [17,18], and in adolescence [19], while others found smaller volumes [20]. Padilla et al. [18] found that preterm infants without focal brain lesions have decreased CoGM volume over the whole brain, but increased grey matter volumes in the occipital lobes.

It has been described that white matter injury (the most common type of brain injury in preterm infants), varying from cystic periventricular leukomalacia, punctate unmyelinated white matter (UWM) lesions, to diffuse UWM injury, may have secondary maturational and trophic consequences due to axonal damage, affecting the microstructural integrity and connectivity between thalamus and cortex [3,4]. This might disturb the early formation, development and maturation of the cerebral cortex.

Magnetic resonance imaging (MRI) is of additional value in indicating infants at the highest risk of neurodevelopmental impairments. Quantitative assessment of cortical development based on MRI, describing volume, cortical surface area, cortical thickness, and cortical folding could potentially aid in evaluating development. These quantitative descriptors and their longitudinal change are interesting when investigated in specific brain regions, in infants with normal development, as well as in cases with brain injury. Altered cortical development of preterm infants has been mainly reported at term equivalent age, childhood, or adolescence [10,18,19,21]. Longitudinal imaging prior to term equivalent age, when most changes take place, is lacking.

The aim of this study is to quantitatively describe morphological changes of the cerebral cortex in a unique cohort of extremely preterm infants with and without brain injury, with clinically acquired longitudinal MR images at 30 and 40 weeks postmenstrual age (PMA).

Data

This study included 117 longitudinally scanned preterm infants. After exclusion of 17 infants who had at least one image of non-diagnostic quality, e.g. due to movement artefacts, and 15 infants with severe brain injury resulting in inaccurate automatic segmentations, a set of 85 infants, with good quality longitudinal images, remained. These infants had an average gestational age of 26.6 ± 1.0 weeks at birth (range: 24.4—27.9 weeks), were 30.7 ± 0.8 week PMA (range: 28.7—32.7 weeks) at the first scan, and 41.1 ± 0.5 weeks PMA (range: 40.0—42.7 weeks) at the second scan. Imaging was performed in accordance with standard clinical practice at the Neonatal Intensive Care Unit of the Wilhelmina Children's Hospital of the University Medical Center Utrecht, The Netherlands. Detailed patient information is listed in Table 1. All patients were sedated with oral chloral hydrate (30—60 mg/kg). Coronal T_2-weighted images were acquired on a Philips Achieva 3T scanner (Philips Medical Systems, Best, The Netherlands)

Table 1. Patient information and the number of patients with brain injury in this cohort.

Number of patients	85
Male/female	42/43
Intraventricular haemorrhage grade I	10 (11.8%)
Intraventricular haemorrhage grade II	13 (15.3%)
Intraventricular haemorrhage grade III	5 (5.9%)
Posthaemorrhagic ventricular dilation	4 (4.7%)
Punctate white matter lesions (> 6)	2 (2.4%)
Cerebellar lesions (> 6) or cerebellar haemorrhage	3 (3.5%)
Lenticulostriate infarction	3 (3.5%)

No patients with cystic periventricular leukomalacia and no patients with periventricular haemorrhagic infarction were found in this cohort.

doi:10.1371/journal.pone.0131552.t001

with multislice 2D turbo spin echo sequences, using an echo time of 120 ms at 30 weeks and 150 ms at 40 weeks, and a repetition time of 10085 ms at 30 weeks and 4847 ms at 40 weeks. The images were reconstructed to voxel sizes of $0.34 \times 0.34 \times 2.0$ mm^3 at 30 weeks PMA and $0.35 \times 0.35 \times 1.2$ mm^3 at 40 weeks PMA.

Permission from the medical ethical review committee of the University Medical Center Utrecht (MERC UMC Utrecht) for the current study and informed parental consent for the MRI was obtained. Patient data were anonymised prior to the analysis. Since this was a retrospective study, using MR images performed as part of standard clinical care, oral consent for the MRI was obtained by the treating physician and any questions or remarks were noted in the charts. No written consent was deemed necessary. The MERC UMC Utrecht waived the need for parental consent for both the use of medical data and for publication of medical images.

All MR images acquired at 40 weeks PMA were scored for brain injury using the assessment tool presented by Kidokoro et al. [2]. This scoring system evaluated unmyelinated white matter abnormality, cortical grey matter abnormality, deep grey matter abnormality, cerebellar abnormality, and total brain abnormality. It included visual assessment as well as manual 2D measurements.

Based on the score, the patients were divided in four classes: normal, mild, moderate, and severe. For total brain abnormality this resulted in: 35 patients in the normal class, 42 in the mild class, 7 in the moderate class, 1 in the severe class. For CoGM abnormality this resulted in: 27 patients in the normal class, 35 in the mild class, 18 in the moderate class, and 5 in the severe class. Because of the small number of patients in the severe classes, the moderate and severe classes were combined in the statistical evaluation.

The interhemispheric fissure width, which was part of the cortical grey matter abnormality score, is recognised as a measure of cerebral atrophy [22] and is therefore also investigated separately.

Methods

To enable analysis of the cortex, UWM, CoGM, and cerebrospinal fluid in the extracerebral space (CSF) were automatically segmented in the coronal T$_2$-weighted images. Subsequently, the brain was divided into frontal, temporal, parietal, and occipital lobes. Finally, the automatic segmentations and parcellations were used to calculate quantitative descriptors characterising cortical development in the whole cohort. A pilot study using these quantitative descriptors has been described by Moeskops et al. [23].

3.1. Segmentation and parcellation

UWM, CoGM and CSF were automatically segmented in the coronal T_2-weighted images using a recently presented supervised classification method [24]. The method has been evaluated in the Neonatal Brain Segmentation challenge (NeoBrainS12), a study comparing the performance of algorithms for automatic neonatal brain segmentation [25]. The results on images acquired with the same protocol as used in this study are available at http://neobrains12.isi.uu.nl/mainResults.php and show better performance of this method compared to other methods. An example of a CoGM segmentation result in images acquired at 30 and 40 weeks PMA of the same patient is illustrated in Fig 1.

To enable localised analysis, we have automatically parcellated both the right and the left hemisphere of the MR brain images into frontal, temporal, parietal, and occipital lobes, i.e. eight regions, using registration of an annotated template image. An example of a resulting automatic parcellation for the images acquired at 30 and 40 weeks PMA is shown in Fig 2. Details of this procedure can be found in S1 Methods.

3.2. Quantification of cortical morphology

Based on the automatic segmentation results, several quantitative descriptors were computed. No further topological correction [26] was performed before these computations. UWM, CoGM, and CSF volumes were determined, and the inner and outer CoGM surface areas were estimated using a voxel-based approach that assigns a weight to each voxel on the surface based the configuration of its neighbouring voxels [27]. Furthermore, cortical thickness was computed in 3D following the method described by Jones et al. [28]. Cortical folding was quantified using two different methods: by gyrification index [29] in 3D, and by global mean curvature. The gyrification index was computed as the ratio between the inner CoGM surface and a
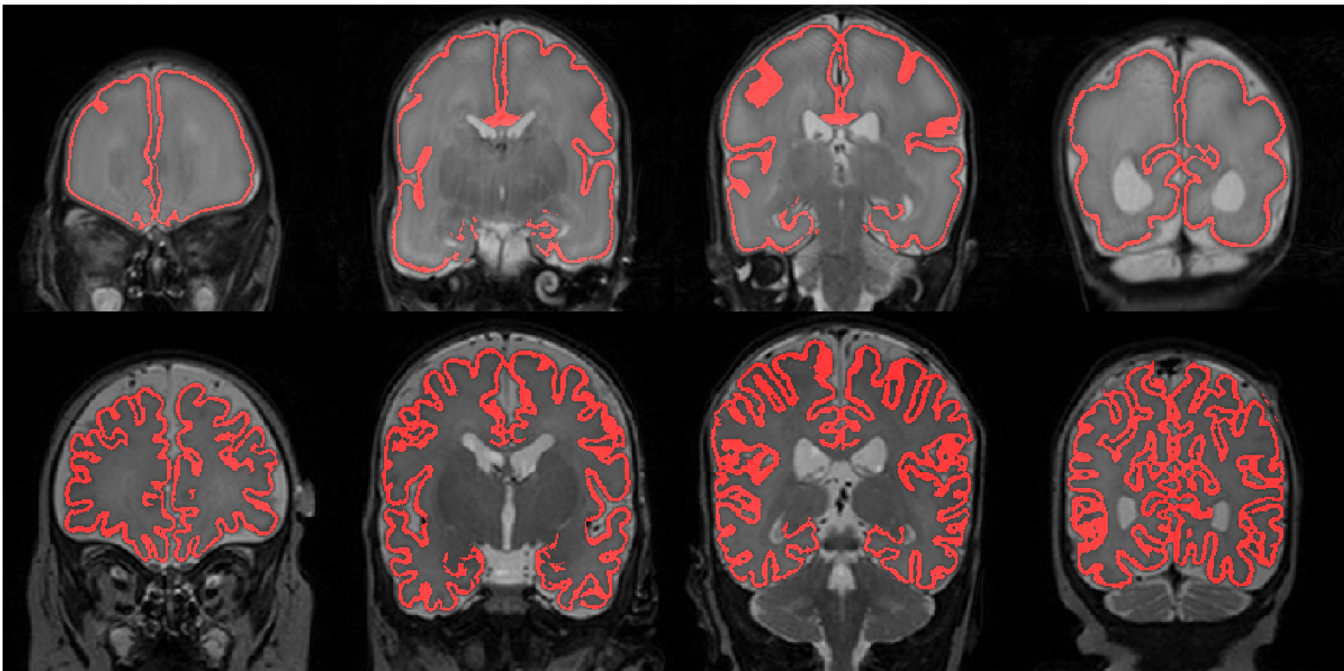

Fig 1. Automatic segmentation of CoGM at 30 (top) and 40 weeks PMA (bottom) for the same patient, shown in four slices of the T2-weighted images. Note that, because of the limited resolution, CSF inside the sulci was not always visible, which resulted in local overestimation of cortical thickness.
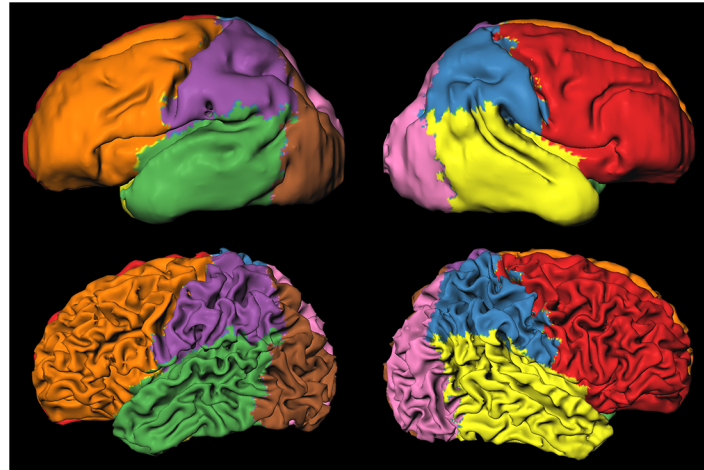
doi:10.1371/journal.pone.0131552.g001

Fig 2. Automatic parcellation of the images acquired at 30 weeks (top) and 40 weeks (bottom) in frontal (red and orange), temporal (yellow and green), parietal (blue and purple), and occipital (pink and brown) lobes. The images were scaled separately and therefore do not show change in size of the brain.

smooth convex hull segmentation [30] around the UWM segmentation. Global mean curvature was computed by normalised summation [31] of the local mean curvature of the inner and outer CoGM surface combined. An example of the local mean curvature of the inner CoGM surface is shown in Fig 3. Details of these methods can be found in S1 Methods.

These descriptors were computed for the whole brain as well as for each of the brain regions, for the images acquired at 30 weeks PMA as well as for the images acquired at 40 weeks PMA. To evaluate the change between 30 and 40 weeks PMA, longitudinal increase factors were computed for each patient as the ratio between the descriptors at 40 and 30 weeks PMA.
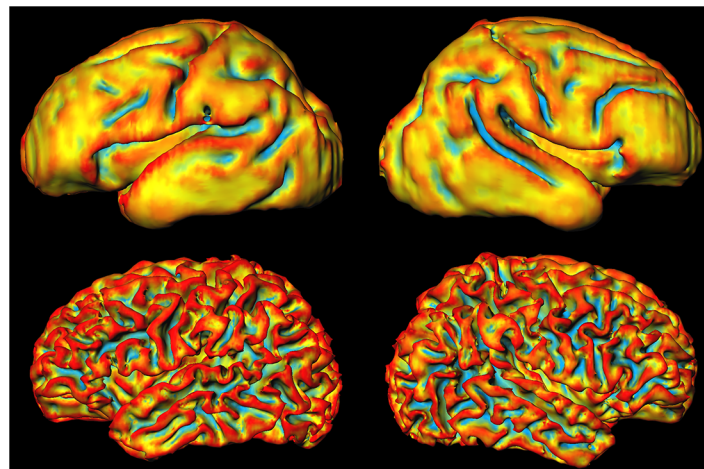

Fig 3. Local mean curvature of the inner cortical surface as obtained by automatic segmentation on the images acquired at 30 weeks PMA (top) and at 40 weeks PMA (bottom) for one patient. Red indicates positive curvature, blue indicates negative curvature, and yellow indicates zero curvature. The images were scaled separately and therefore do not show change in size of the brain.

3.3. Statistical evaluation

To evaluate whether the descriptors show differences between the brain regions, differences between the abnormality classes, or differences with respect to the development between 30 and 40 weeks PMA, linear mixed modelling was used to estimate these effects for the descriptors computed from the images acquired at 30 and 40 weeks PMA and from their longitudinal increase factors. The statistical evaluation was performed in R (version 3.1.1).

Models were made, per descriptor, for the images acquired at 30 weeks PMA, the images acquired at 40 weeks PMA, and the longitudinal increase factors separately. Categorical variables were used to describe the hemispheres, the lobes and the abnormality scores. To correct for differences in age at the time of scanning, the patient age at the time of the scan was included in the models for the images acquired at 30 weeks, and the time interval between the two scans was included in the models for the increase factors. No influence of age at the time of scanning was found for the images acquired at 40 weeks, so age was not included in those models. Model optimisation was performed based on Akaike's information criterion [32].

Results

The results are presented for: the images acquired at 30 weeks PMA, the images acquired at 40 weeks PMA, as well as the longitudinal changes between these two time points. The first subsection of the results presents the global quantitative descriptors evaluated over the whole brain, while the second subsection presents these descriptors evaluated per region. In the third subsection, the descriptors are presented in relation to the abnormality score classes.

4.1. Global evaluation

Fig 4 shows descriptors evaluated over the whole brain versus PMA at the time of scanning, while Table 2 lists the average values and their increase factors. In a period of 10.4 ± 1.0 weeks (mean ± standard deviation) the outer UWM surface area (i.e. inner CoGM surface area) increased by a factor of 3.7, while the UWM volume increased by 1.9. The outer CoGM surface area increased by a factor of 3.3, and the CoGM volume increased by a factor of 4.6. Cortical folding increased by factor 1.9, both in terms of gyrification index and in terms of the global mean curvature of the inner and outer surface. Furthermore, median cortical thickness increased by a factor of 1.3.

4.2. Regional evaluation

Fig 5 shows boxplots for all regional descriptors in ten regions: the right and left hemispheres, as well as the right and left frontal, temporal, parietal, and occipital lobes. The average increase factors between 30 and 40 weeks PMA for these regions are shown in Fig 6. The results of the statistical evaluation obtained with linear mixed modelling can be found in S1, S2 and S3 Tables.

Evaluation of the calculated descriptors per lobe revealed that the brain does not develop equally over all regions. For the images acquired at 30 weeks PMA, lower median cortical thickness, gyrification index, and global mean curvature were found for the occipital lobes than for the whole hemispheres, but these values were higher for the images acquired at 40 weeks PMA. Furthermore, compared to the whole hemispheres, higher median cortical thickness, gyrification index, and global mean curvature were obtained for the parietal lobes at 30 weeks PMA, as well as higher values for median cortical thickness, and gyrification index at 40 weeks PMA. When the increase factors of these descriptors between 30 and 40 weeks PMA were compared (Fig 6), larger increase was found in the occipital lobes for UWM volume, inner cortical surface
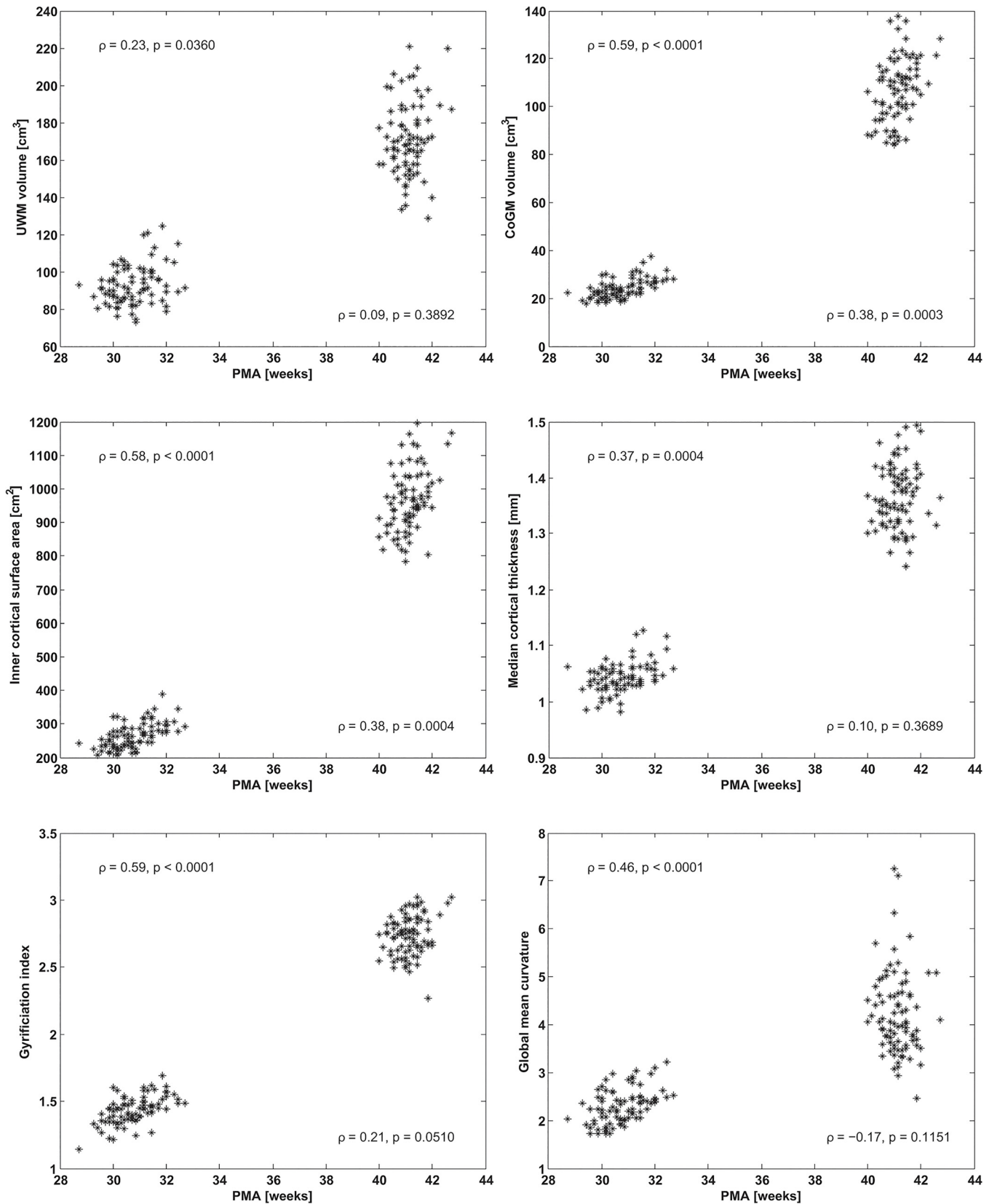
Fig 4. UWM volume (top left), CoGM volume (top right), inner cortical surface area (middle left), median cortical thickness (middle right), gyrification index (bottom left), global mean curvature (bottom right), for the images acquired at 30 and 40 weeks PMA, shown versus PMA at the time of scanning. Spearman's rank correlation coefficients (ρ) and the corresponding p-values are shown for 30 (left) and 40 weeks PMA (right) separately.

doi:10.1371/journal.pone.0131552.g004

area, median cortical thickness, gyrification index, and global mean curvature. These findings indicate that more rapid development took place in the occipital part of the brain for all these descriptors between 30 and 40 weeks PMA than over the whole hemispheres. The parietal lobes showed larger increase factors for inner cortical surface area, median cortical thickness, and gyrification index. The temporal lobes only showed larger increase factors for median cortical thickness, and the frontal lobes only for UWM volume and global mean curvature.

4.3. Comparison with abnormality scores

In Fig 7 the global cortical descriptors computed from the images acquired at 30 and 40 weeks PMA are shown per brain abnormality class. The effects for the patients in these abnormality classes based on linear mixed modelling are listed in Table 3. Fig 8 shows that the cortical descriptors acquired at 40 weeks PMA were significantly correlated with the interhemispheric fissure width, which is part of the CoGM abnornormality scoring and is recognised as a measure of cerebral atrophy [22]. No significant correlation with interhemipheric fissure width was found for the images acquired at 30 weeks PMA.

Overall, median cortical thickness increased with increasing abnormality score, while gyrification index and global mean curvature decreased with increasing abnormality score. Using α = 0.05, we found a significant increase in median cortical thickness for the images acquired at 40 weeks PMA when comparing the combined moderate and severe CoGM abnormality class with the normal class (no abnormality). For the gyrification index, significant decreases were found when comparing the mild class and the combined moderate and severe abnormality class with the normal class, for total brain abnormality as well as for CoGM abnormality. For global mean curvature, a significant decrease was found when comparing the combined moderate and severe CoGM abnormality class with the normal class. For the images acquired at 30 weeks PMA, significant decreases in gyrification index were found for the mild and the combined moderate and severe total brain abnormality classes compared with the normal class, and a significant decrease in global mean curvature was found for the mild total brain abnormality class compared with the normal class. The same patterns were visible from the

Table 2. Mean (μ) and corresponding standard deviation (σ) for the descriptors acquired at 30 and 40 weeks PMA, and their longitudinal increase factors.

Descriptor	30 weeks PMA ($\mu \pm \sigma$)	40 weeks PMA ($\mu \pm \sigma$)	Increase factor ($\mu \pm \sigma$)
UWM volume	93 ± 11 cm^3	171 ± 19 cm^3	1.9 ± 0.2
CoGM volume	24 ± 4 cm^3	107 ± 13 cm^3	4.6 ± 0.7
CSF volume	53 ± 9 cm^3	120 ± 22 cm^3	2.3 ± 0.6
Inner cortical surface area	264 ± 38 cm^2	964 ± 91 cm^2	3.7 ± 0.4
Outer cortical surface area	277 ± 39 cm^2	894 ± 104 cm^2	3.3 ± 0.5
Median cortical thickness	1.0 ± 0.0 mm	1.4 ± 0.1 mm	1.3 ± 0.1
Gyrification index	1.4 ± 0.1	2.7 ± 0.1	1.9 ± 0.1
Global mean curvature	2.3 ± 0.4	4.2 ± 0.9	1.9 ± 0.5

The computed descriptors were: UWM volume, CoGM volume, CSF volume, inner cortical surface area, outer cortical surface area, median cortical thickness, gyrification index, and global mean curvature of the inner and outer cortical surface together.
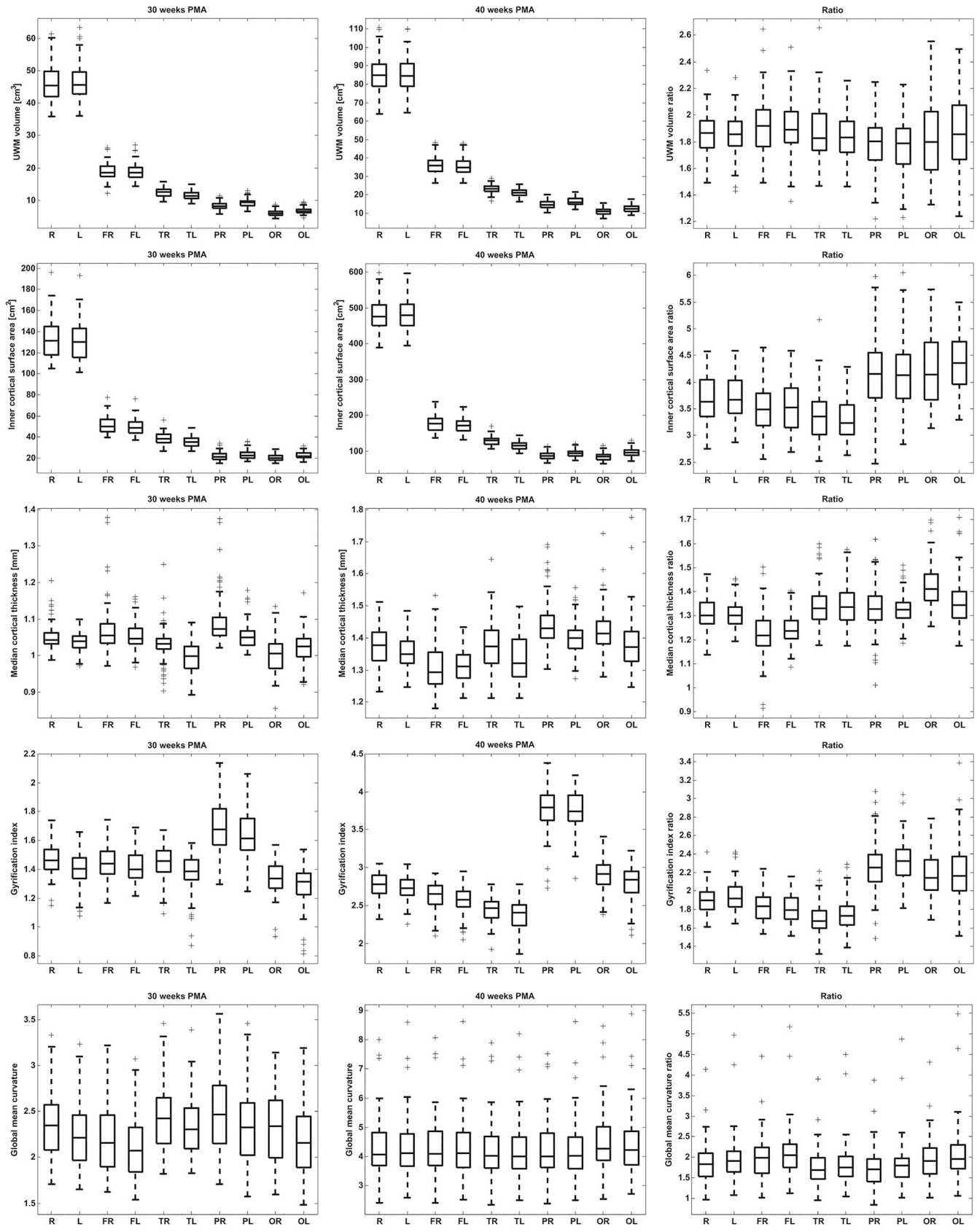
doi:10.1371/journal.pone.0131552.t002

Fig 5. Regional evaluation (in terms of standard boxplots) for, from top to bottom: UWM volume, inner cortical surface area, median cortical thickness, gyrification index, and global mean curvature. The columns show, from left to right: the results for the images acquired at 30 weeks, the results for the images acquired at 40 weeks, and the ratio between the results for the images acquired at 40 and 30 weeks. Note that, for the descriptors acquired at 30 and 40 weeks PMA, UWM volume and inner cortical surface area were dependent of the size of the defined regions of the parcellation, while median cortical thickness, gyrification index, and global mean curvature were independent of size. In every frame the results are shown for the right (R) and left (L) hemispheres, the right (FR) and left (FL) frontal lobes, the right (TR) and left (TL) temporal lobes, the right (PR) and left (PL) parietal lobes, and the right (OR) and left (OL) occipital lobes.
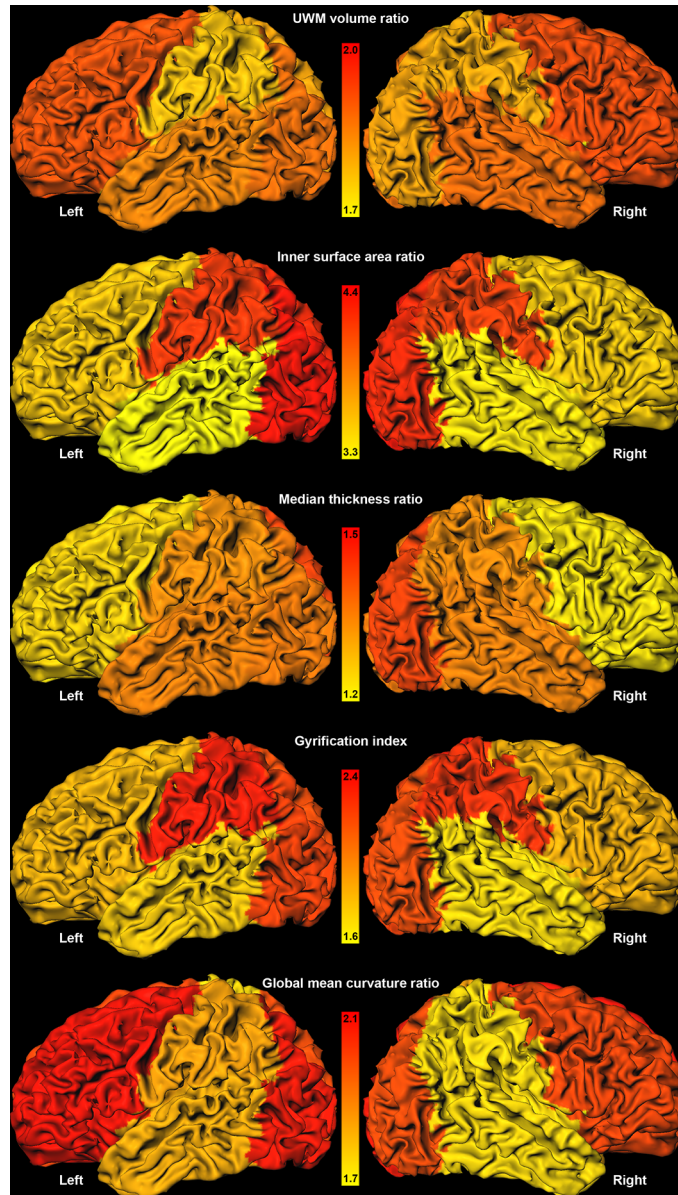
doi:10.1371/journal.pone.0131552.g005

Fig 6. Average regional increase factors for both hemispheres visualised on the inner cortical surface of one randomly chosen patient. The highest increase factor is shown in red and the lowest increase factor is shown in yellow; the range was set separately per descriptor. Note that this figure provides a visualisation of the data in the last column of Fig 5.
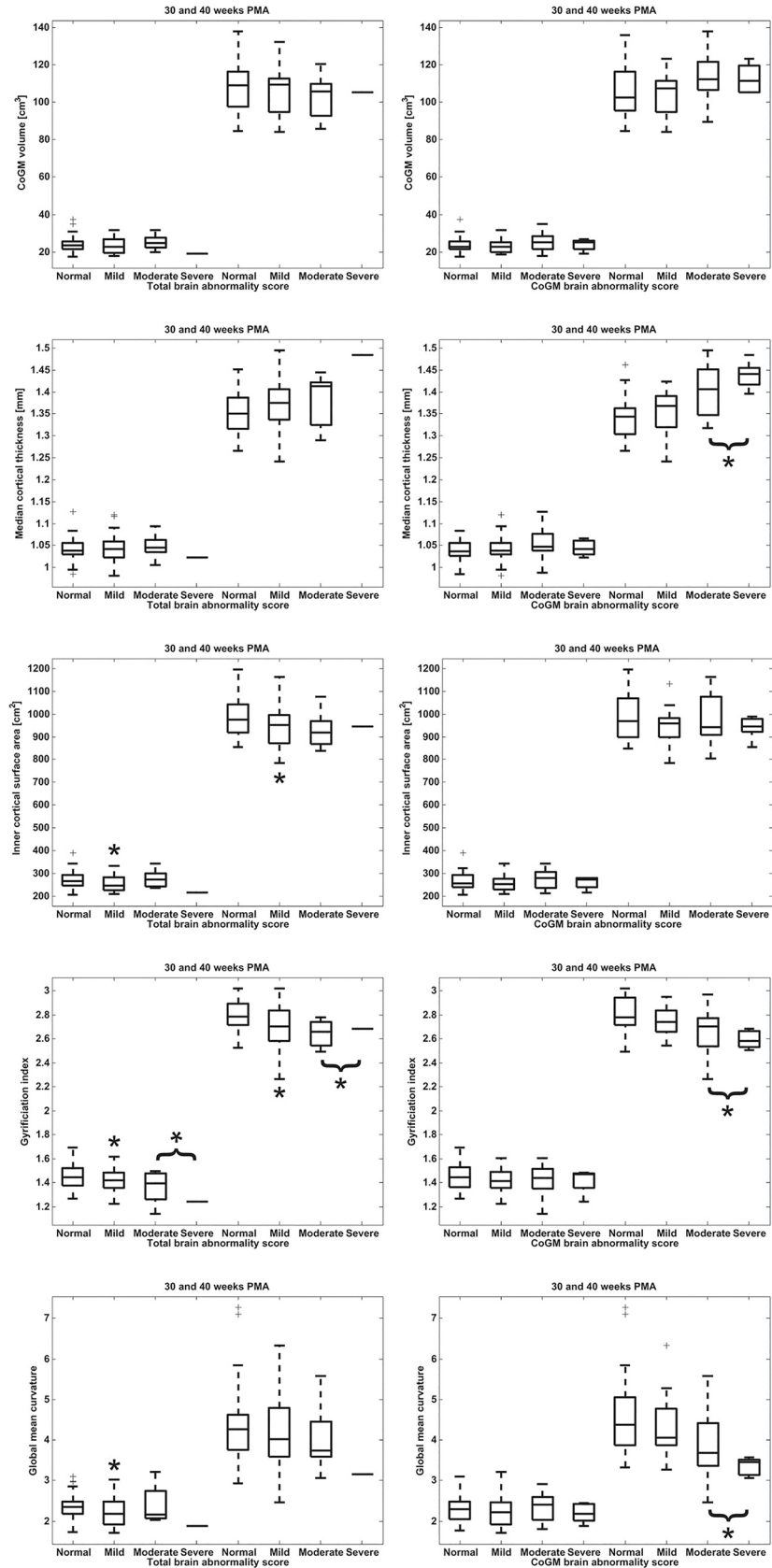
doi:10.1371/journal.pone.0131552.g006

Fig 7. Global cortical morphology descriptors computed from the images acquired at 30 (left) and 40 weeks PMA (right), as a function of total brain (left column) and CoGM abnormality score (right column). From top to bottom: CoGM volume, median cortical thickness, inner cortical surface area, gyrification index, global mean curvature. The four abnormality classes are (i) normal, (ii) mild abnormality, (iii) moderate abnormality, (iv) severe abnormality. Note that there is only one subject in the severe class for the total brain abnormality score. In the statistical evaluation the moderate and severe classes were combined for both the total brain abnormality scoring and the CoGM abnormality scoring. Significant differences with the normal class are indicated with an asterisk (*).

doi:10.1371/journal.pone.0131552.g007

longitudinal increase factors between 30 and 40 weeks PMA. No significant influence of UWM abnormality score was found on the descriptors.

Discussion

This paper evaluated UWM volume, CoGM volume, CSF volume, inner and outer cortical surface area, median cortical thickness, gyrification index, and global mean curvature in preterm infants with longitudinal imaging. These descriptors have been previously related to the state of the brain development [5,6,10,30,31,33–40], but thus far, they have not been investigated in early longitudinal imaging of preterm infants. In agreement with previous findings in cross-sectional studies, this study showed an increase of all evaluated descriptors between 30 and 40 weeks PMA. Significantly more rapid development occurred in the occipital lobes than in other regions. Interestingly, a significant increase in cortical thickness and a significant decrease in cortical folding (in terms of gyrification index and global mean curvature) were found in infants with higher brain abnormality scores according to Kidokoro et al. [2]. These effects were more apparent at 40 weeks PMA than at 30 weeks PMA. The results for gyrification index and global mean curvature indicated agreement between the descriptors that were

Table 3. Effects of abnormality classes, relative to the normal class, on median cortical thickness, inner cortical surface area, gyrification index, and global mean curvature, computed from the images acquired at 30 and 40 weeks PMA, estimated with linear mixed modelling.

Descriptor	Abnormality class	Effect on descriptor	*p*-value
Median thickness [mm] (40 weeks PMA)	CoGM: mild	+0.0083	0.5096
	CoGM: moderate and severe	+0.067	<0.0001*
Inner cortical surface area [cm^2] (40 weeks PMA)	Total brain: mild	-8.7	0.0363*
	Total brain: moderate and severe	-11.7	0.0967
Gyrification index (40 weeks PMA)	Total brain: mild	-0.11	0.0011*
	Total brain: moderate and severe	-0.16	0.0075*
	CoGM: mild	-0.07	0.0553
	CoGM: moderate and severe	-0.17	0.0001*
Global mean curvature (40 weeks PMA)	CoGM: mild	-0.29	0.1910
	CoGM: moderate and severe	-0.86	0.0008*
Inner cortical surface area [cm^2] (30 weeks PMA)	Total brain: mild	-3.7	0.0096*
	Total brain: moderate and severe	-2.0	0.3996
Gyrification index (30 weeks PMA)	Total brain: mild	-0.04	0.0362*
	Total brain: moderate and severe	-0.12	0.0002*
Global mean curvature (30 weeks PMA)	Total brain: mild	-0.15	0.0388*
	Total brain: moderate and severe	-0.06	0.6447

No significant effects of the abnormality score were found for CoGM volume. Significant differences with the normal class are indicated with an asterisk (*), if none of the classes showed a significant effect the descriptor is not shown in this table.
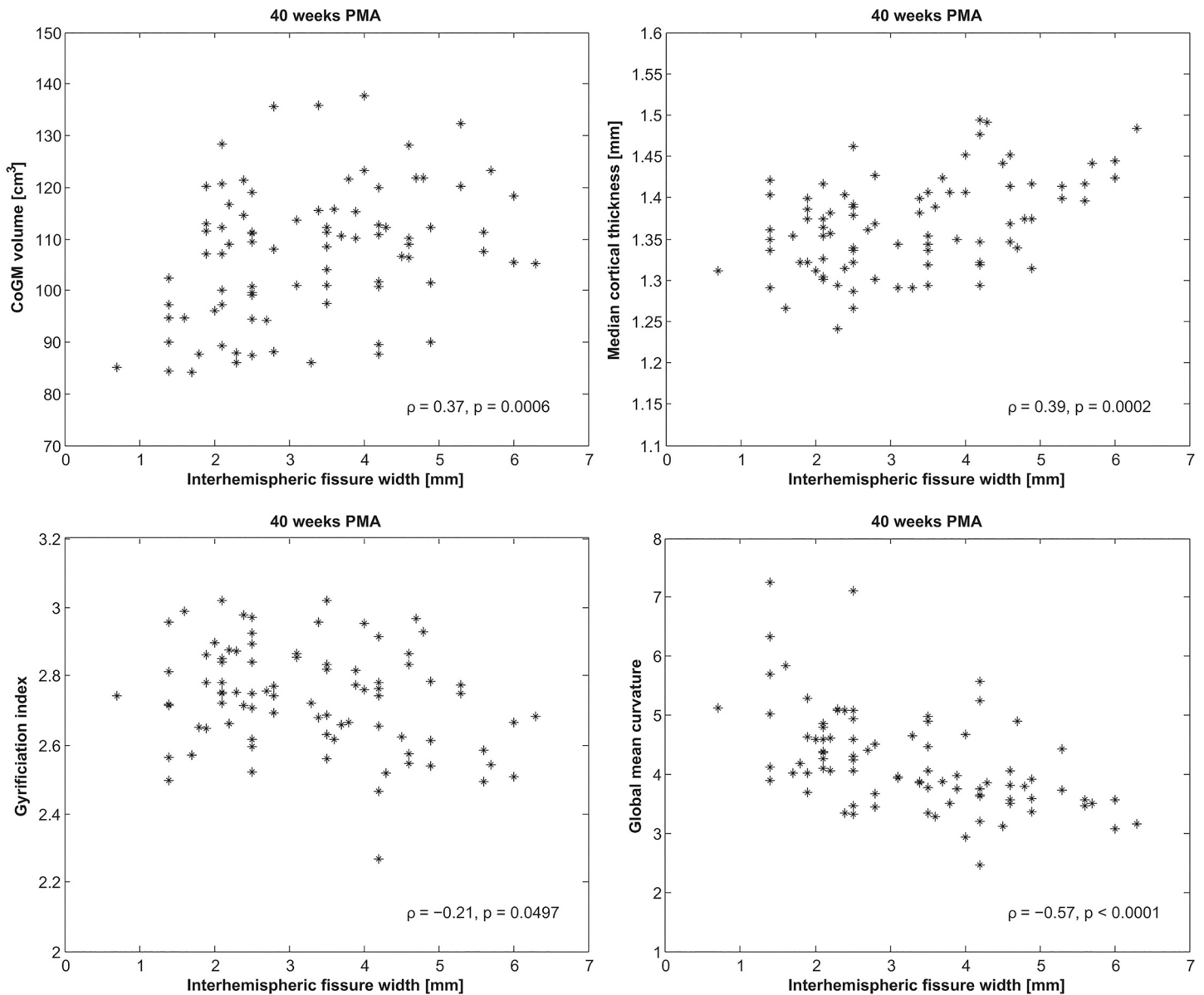
doi:10.1371/journal.pone.0131552.t003

Fig 8. CoGM volume, median cortical thickness, gyrification index, and global mean curvature computed from the images acquired at 40 weeks PMA versus the width of the interhemispheric fissure, measured between the crowns of the superior frontal gyri. Spearman's rank correlation coefficients (ρ) and the corresponding *p*-values are shown at the bottom right. No significant correlation was found for inner cortical surface area.

automatically extracted from the images and visual scoring, as delayed gyrification is included in the CoGM abnormality scoring.

5.1. Global brain development

Cross-sectional studies of similar cortical descriptors with preterm neonatal [31,33], as well as foetal MRI [36,41,42], showed an association with age. In our current study, clear increases between 30 and 40 weeks PMA were found for all descriptors (Fig 4). An association with PMA at the time of scanning was found for the images acquired around 30 weeks PMA. This effect was less visible in the images acquired around 40 weeks PMA. This could indicate that

the extra-uterine environment, or other consequences of preterm birth, did not yet show an effect on cortical development at 30 weeks PMA, but did have an effect between 30 and 40 weeks PMA, resulting in a larger range of the descriptors at 40 weeks PMA, depending on postnatal complications. Additionally, cortical development occurs less rapidly around 40 weeks PMA than around 30 weeks PMA [36], resulting in a less strong influence of PMA at the time of scanning on the descriptors at 40 weeks PMA than at 30 weeks PMA. No influence of the gestational age at birth was found on the cortical descriptors for the patients in this study.

To compare the difference between development of preterm infants and normal foetal development, analysis of control images of healthy newborns needs to be performed. Unfortunately these data are not available, since no ethical approval has been obtained to scan healthy newborns in our institution so far. Wright et al. [36] recently evaluated different global curvature descriptors applied to foetal MR brain images acquired between 21 and 39 weeks gestational age. With increasing age, similar increases in these descriptors were shown. This study did, however, not evaluate cortical thickness.

5.2. Regional brain development

At 40 weeks PMA, the occipital lobes were more mature than the frontal and temporal lobes in terms of gyrification index and global mean curvature. When the increase factors between 30 and 40 weeks PMA were considered, the largest change took place in the occipital lobes. These results are in agreement with the literature suggesting that brain development takes place in an occipital-frontal direction [43–46], which was confirmed by *in vivo* studies [47–50]. The more rapid development in the occipital lobes could explain the earlier functional use and activity of the visual system in preterm infants [18,51,52], in contrast to e.g. behavioural functions involving the frontal lobes. This is supported by previous work suggesting that early neuronal activity of preterm infants relates to subsequent brain growth [53]. Consequently, rapid occipital development could make this region more vulnerable and might be an explanation for the high risk of visual dysfunction in preterm infants [54,55].

The right hemisphere was significantly more mature than the left hemisphere in terms of gyrification index for the images acquired at 30 weeks PMA, as well as the images acquired at 40 weeks PMA. For global mean curvature this was only visible for the images acquired at 30 weeks PMA. This difference between hemispheres corresponds to previous findings in the literature suggesting that the right hemisphere presents gyral complexity earlier than the left hemisphere [33,56].

5.3. Cortical development and brain injury

An interesting finding was that patients with a higher (CoGM) abnormality score had increased cortical thickness and decreased cortical folding in terms of gyrification index and global mean curvature. The difference in thickness is significant, however, it is small: on average 1.3 vs. 1.4 mm for the images acquired at 40 weeks PMA, given a voxel size of 0.35 mm. This is a subvoxel difference and therefore difficult to interpret and evaluate visually. Additionally, in this population a positive association was observed between cortical thickness and interhemispheric fissure width measured in 2D (Fig 8), which is part of the CoGM scoring. Cerebral atrophy, expressed as increased hemispheric fissure width, could be a consequence of diffuse UWM injury, with injury to premyelinating oligodendrocytes (preOLs) and a deficit in latemigrating γ-aminobutyric acidergic (GABAergic) neurons. GABAergic neurons are important contributors to the thickness of the upper cortical layers [3,4,45,57,58]. Therefore, disturbed or incomplete migration might appear in the images as a less clear distinction between intensities of UWM and CoGM, which could result in larger cortical thickness estimates. Nosarti et al.

[19] investigated tissue volumes of preterm infants measured in adolescence, and suggested that extensive plastic processes might occur to compensate for brain injury, resulting in increases as well as decreases in CoGM volumes in different regions of the brain.

No significant effect of brain abnormality on CoGM volume was found in this study. The opposing relations of brain injury on cortical folding and cortical thickness obtained in this study might be the reason for different findings reported in the literature with respect to CoGM volume in relation to brain abnormalities [17,18,20]. CoGM volume is influenced by cortical surface area, thus by cortical folding, as well as cortical thickness. As suggested by earlier literature and by the results of our study, increase in cortical thickness might indicate disruption of brain development, whereas increase in cortical folding might indicate good development. Therefore, these two counteracting effects on volume could lead either to no visible volume differences, or to differences in either direction, depending on which of the effects is stronger. Hence, CoGM volume alone is likely not a good indicator of cortical development.

The associations of the descriptors with the abnormality scores were less clearly visible for the images acquired at 30 weeks PMA. This corresponds to the previously mentioned larger range of the descriptors acquired at 40 weeks PMA (Fig 4), showing larger deviations in development than when imaged at 30 weeks PMA, likely influenced by the extra-uterine conditions. A critical part of brain development takes place between 30 and 40 weeks PMA and disturbances such as white matter injury can therefore have a large influence on development, i.e. result in secondary brain damage. PreOLs are especially vulnerable to hypoxia-ischemia and inflammation, which are well known processes for white matter injury in preterm infants. As a result of cell death of preOLs, early oligodendrocyte progenitors proliferate and differentiate rapidly, but fail to myelinate normally, ultimately resulting in disrupted development of the cortex as well [59,60]. This damage requires time to develop and become visible and hence the influence on cortical development would be more apparent at 40 weeks PMA. This means that the period between 30 and 40 weeks PMA might offer a window of opportunity for neuroprotective interventions.

No significant influence of UWM abnormality scoring was found on these descriptors. However, interhemispheric fissure width did show a correlation with the cortical descriptors, which might indicate atrophy, possibly due to diffuse UWM injury. Diffuse UWM injury, which is difficult to visualise with conventional imaging, is nevertheless known to influence cortical development [60]. This was further supported by significant differences, in terms of gyrification index and global mean curvature, between normal and mild abnormality scores (Fig 7), indicating that mild injury, possibly involving diffuse UWM injury, might have had an influence on cortical development as well.

The processes behind the development of the cerebral cortex are not yet fully understood. Suggested factors include: genetics [61,62], neuronal differentiation [63–65] and mechanical effects [66–70]. However, in the ferret brain, gyrification seems to arise secondary to cortical processes involving neuronal differentiation [71]. With respect to these mechanical effects, Toro and Burnod [68] have suggested a morphogenetic model of cortical folding in which cortical growth can induce cortical folding by itself. In contrast to this, another theory suggests that specific location and shape of sulci are determined by visco-elastic tensions from white matter tracts connecting cortical regions [67,69,70]. The latter theory might explain why specific abnormalities in the cortical sulcal pattern are observed in certain brain developmental disorders in preterm infants [72–74]. These cortical abnormalities might be a consequence of subtle impairments in neuronal migration and cortico-cortical connections.

In the foetal sheep brain, Rees et al. [75] confirmed delayed gyral formation at mid-gestation caused by sub-acute hypoxemia, an underlying pathophysiological mechanism often described in preterm infants. It is often hypothesised that the disability in preterm infants is primarily

associated with impaired neural connectivity with or without tissue loss or visible WMI. Dean et al. [76] found that in the foetal sheep brain reversible cerebral ischemia, even without neuronal loss, showed significant diffuse failure of maturation of cortical pyramidal neurons. This was associated with impaired dendritic growth and synapse formation, consistent with altered connectivity. Delayed decline in cortical fractional anisotropy (FA) on MRI was associated with these changes.

Ball et al. [77] reported that preterm infants at term-equivalent age, in the absence of severe white matter injury, showed a loss of microstructural integrity of the connective white matter tracts. Very preterm infants exhibit cortical neuroplasticity due to reduced thalamo-cortical connectivity compared with term-born controls. Clinical and experimental studies are showing that early WMI is associated with a reduction in cortical complexity. It seems that grey matter damage due to loss of connections, rather than cell loss, plays a major factor in long-term disability [78]. Whether disturbances in connectivity, without visible UMW abnormalities, are related with developmental delay of cortical folding is unclear. Longitudinal MRI studies quantifying cortical development and changes in connectivity with long-term follow-up will provide more insight.

5.4. Limitations

The presented study has several limitations. First, the resolution of the acquired images is limited, which resulted in regions where the CSF inside the sulci was not always visible. Therefore, the outer cortical surface, i.e. the surface between CoGM and CSF, was not always well recognised in these regions. This can also be seen from the average outer cortical surface area computed at 40 weeks PMA (Table 2), which is smaller than the average inner cortical surface area. Cortical thickness in these regions was therefore sometimes overestimated as well. To reduce the influence of this effect on the global descriptors for cortical thickness, median values have been presented. In addition to this, cortical thickness is difficult to estimate based on MRI because of the ongoing development of the cortex [79]. Second, the evaluated descriptors were computed fully automatically from the images. This allowed analysis of a large set of images, but could generate errors human observers do not make. However, the performance of the applied segmentation method was similar to inter-observer variability as shown in the Neo-BrainS12 study [25], which suggests that these errors were minimal, and therefore not likely to have had a large influence on the computed descriptors. Third, it should be noted that the descriptors used in this study cannot be directly compared across studies, because they are influenced by several factors such as the acquisition protocol, the segmentation method, the definition of the tissue types, the definition of the descriptors, and details of the implementation. A wide range of values was reported in studies that included patients within the same age range (including studies with foetal imaging and term-born infants). For inner CoGM surface area, the values range from 150 to 1500 cm^2 [30,31,33,34,37,80]. In our study the average surface area increases from 264 to 964 cm^2 (Table 2). The computation of the cortical surface area is highly dependent on the scale of measurement (this is commonly referred to as the *coastline paradox*), which could, in addition to the above mentioned factors, explain the large range of values in the literature. For cortical thickness, values between 1.2 to 1.4 mm were found by Xue et al. [80]. In our study the average cortical thickness increased from 1.0 to 1.4 mm (Table 2). For gyrification index, values between 1.1 and 2.2 were reported [31,40]. In our study the average gyrification index increased from 1.4 to 2.7 (Table 2), which is larger than found in the mentioned studies. These studies also report a lower cortical surface area, which could suggest that they are based on a smoother definition of the cortical surface, which directly influences the gyrification index as well. For global mean curvature, values from 2 to 10 were reported

[31,36], based on several definitions. In our study the average global mean curvature increased from 2.3 to 4.2 (Table 2). Fourth, the number of patients in the severe abnormality class was small. Therefore, statistical conclusions were drawn for patients in the combined moderate and severe class. Finally, our work analysed longitudinally acquired images at fixed time points, while other studies [31,33,36] focused on single images of patients acquired cross-sectionally at different ages. Our study did not allow the analysis of the development over the full age range, but the strength of this approach was that it did allow us to evaluate the (regional) change of the quantitative descriptors within a patient.

Conclusion

The presented study, automatically quantifying cortical development, provides insight in regional and longitudinal development based on T_2-weighted MR brain images of preterm infants with and without brain injury, longitudinally acquired at 30 and 40 weeks PMA. The evaluated descriptors showed a larger change in the occipital lobes than in the other lobes. Interestingly, increased cortical thickness and decreased cortical folding were found in infants with brain injury scored according to a conventional abnormality scoring system. This was more pronounced at 40 weeks PMA than at 30 weeks PMA, suggesting that the cortical maturation processes during these 10 weeks might be affected by brain injury or other consequences of preterm birth. This might offer a window of opportunity for neuroprotective intervention. The potential of these findings to predict long-term cognitive outcome and the effect of specific clinical risk factors should be evaluated in further studies.

Supporting Information

S1 Methods. Additional information about the methods.
(DOC)

S1 Table. Regional effects for the images acquired at 30 weeks PMA, estimated with linear mixed modelling. The effects are relative to the estimated value over the left hemisphere. If there was an additional right-left difference for a specific lobe, this was modelled as an interaction. Note that UWM volume and inner cortical surface area were dependent of the size of the defined regions of the parcellation, while median cortical thickness, gyrification index, and global mean curvature were independent of size. The age at the time of scanning, as well as the abnormality score were included in the models.
(DOC)

S2 Table. Regional effects for the images acquired at 40 weeks PMA, estimated with linear mixed modelling. The effects are relative to the estimated value over the left hemisphere. If there was an additional right-left difference for a specific lobe, this was modelled as an interaction. Note that UWM volume and inner cortical surface area were dependent of the size of the defined regions of the parcellation, while median cortical thickness, gyrification index, and global mean curvature were independent of size. The abnormality score was included in the models.
(DOC)

S3 Table. Regional effects for the longitudinal increase factor between the images acquired at 30 and 40 weeks PMA, estimated with linear mixed modelling. The effects are relative to the estimated value over the left hemisphere. If there was an additional right-left difference for a specific lobe, this was modelled as an interaction. Note that UWM volume and inner cortical surface area were dependent of the size of the defined regions of the parcellation, while median cortical thickness, gyrification index, and global mean curvature were independent of size. The

time interval between the scans was included in the models.
(DOC)

Acknowledgments

Author Contributions

Conceived and designed the experiments: PM MB MV II. Performed the experiments: PM. Analyzed the data: PM. Contributed reagents/materials/analysis tools: MB KK FG LV. Wrote the paper: PM MB KK FG LV MV II.

References

1. Mangin J-F, Jouvent E, Cachia A. In-vivo measurement of cortical morphology: means and meanings. Curr Opin Neurol. 2010; 23: 359–67. doi: 10.1097/WCO.0b013e32833a0afc PMID: 20489617

2. Kidokoro H, Neil JJ, Inder TE. New MR imaging assessment tool to define brain abnormalities in very preterm infants at term. Am J Neuroradiol. 2013; 34: 2208–14. doi: 10.3174/ajnr.A3521 PMID: 23620070

3. Volpe JJ. The encephalopathy of prematurity—brain injury and impaired brain development inextricably intertwined. Semin Pediatr Neurol. 2009; 16: 167–78. doi: 10.1016/j.spen.2009.09.005 PMID: 19945651

4. Volpe JJ. Brain injury in premature infants: a complex amalgam of destructive and developmental disturbances. Lancet Neurol. 2009; 8: 110–124. doi: 10.1016/S1474-4422(08)70294-1 PMID: 19081519

5. Kapellou O, Counsell SJ, Kennea N, Dyet L, Saeed N, Stark J, et al. Abnormal cortical development after premature birth shown by altered allometric scaling of brain growth. PLoS Med. 2006; 3: e265. doi: 10.1371/journal.pmed.0030265 PMID: 16866579

6. Rathbone R, Counsell SJ, Kapellou O, Dyet L, Kennea N, Hajnal J, et al. Perinatal cortical growth and childhood neurocognitive abilities. Neurology. 2011; 77: 1510–7. doi: 10.1212/WNL.0b013e318233b215 PMID: 21998316

7. Dubois J, Benders M, Borradori-Tolsa C, Cachia A, Lazeyras F, Ha-Vinh Leuchter R, et al. Primary cortical folding in the human newborn: an early marker of later functional development. Brain. 2008; 131: 2028–41. doi: 10.1093/brain/awn137 PMID: 18587151

8. Nagy Z, Lagercrantz H, Hutton C. Effects of preterm birth on cortical thickness measured in adolescence. Cereb Cortex. 2011; 21: 300–6. doi: 10.1093/cercor/bhq095 PMID: 20522538

9. Zubiaurre-Elorza L, Soria-Pastor S. Cortical Thickness and Behavior Abnormalities in Children Born Preterm. PLoS One. 2012; 7: e42148. doi: 10.1371/journal.pone.0042148 PMID: 22860067

10. Mürner-Lavanchy I, Steinlin M, Nelle M, Rummel C, Perrig WJ, Schroth G, et al. Delay of cortical thinning in very preterm born children. Early Hum Dev. 2014; 90: 443–50. doi: 10.1016/j.earlhumdev.2014.05.013 PMID: 24976634

11. Gogtay N, Giedd JN, Lusk L, Hayashi KM, Greenstein D, Vaituzis AC, et al. Dynamic mapping of human cortical development during childhood through early adulthood. Proc Natl Acad Sci USA. 2004; 101: 8174–8179. PMID: 15148381

12. Sowell ER, Thompson PM, Leonard CM, Welcome SE, Kan E, Toga AW. Longitudinal mapping of cortical thickness and brain growth in normal children. J Neurosci. 2004; 24: 8223–31. doi: 10.1523/JNEUROSCI.1798-04.2004 PMID: 15385605

13. Tamnes CK, Ostby Y, Fjell AM, Westlye LT, Due-Tønnessen P, Walhovd KB. Brain maturation in adolescence and young adulthood: regional age-related changes in cortical thickness and white matter volume and microstructure. Cereb Cortex. 2010; 20: 534–48. doi: 10.1093/cercor/bhp118 PMID: 19520764

14. Raznahan A, Shaw P, Lalonde F, Stockman M, Wallace GL, Greenstein D, et al. How does your cortex grow? J Neurosci. 2011; 31: 7174–7. doi: 10.1523/JNEUROSCI.0054-11.2011 PMID: 21562281

15. Thambisetty M, Wan J, Carass A, An Y, Prince JL, Resnick SM. Longitudinal changes in cortical thickness associated with normal aging. Neuroimage. 2010; 52: 1215–23. doi: 10.1016/j.neuroimage.2010.04.258 PMID: 20441796

16. Hogstrom LJ, Westlye LT, Walhovd KB, Fjell AM. The Structure of the Cerebral Cortex Across Adult Life: Age-Related Patterns of Surface Area, Thickness, and Gyrification. Cereb Cortex. 2013; 23: 2521–30. doi: 10.1093/cercor/bhs231 PMID: 22892423

17. Peterson BS, Anderson AW, Ehrenkranz R, Staib LH, Tageldin M, Colson E, et al. Regional brain volumes and their later neurodevelopmental correlates in term and preterm infants. Pediatrics. 2003; 5: 939–48.

18. Padilla N, Alexandrou G, Blennow M, Lagercrantz H, Adén U. Brain Growth Gains and Losses in Extremely Preterm Infants at Term. Cereb Cortex. 2014; 1–9. doi: 10.1093/cercor/bht431

19. Nosarti C, Giouroukou E, Healy E, Rifkin L, Walshe M, Reichenberg A, et al. Grey and white matter distribution in very preterm adolescents mediates neurodevelopmental outcome. Brain. 2008; 131: 205–17. doi: 10.1093/brain/awm282 PMID: 18056158

20. Inder TE, Huppi PS, Warfield S, Kikinis R, Zientara GP, Barnes PD, et al. Periventricular white matter injury in the premature infant is followed by reduced cerebral cortical gray matter volume at term. Ann Neurol. 1999; 46: 755–60. Available: http://www.ncbi.nlm.nih.gov/pubmed/10553993 PMID: 10553993

21. Ajayi-Obe M, Saeed N, Cowan F. Reduced development of cerebral cortex in extremely preterm infants. Lancet. 2000; 356: 1999–2000. Available: http://www.sciencedirect.com/science/article/pii/S0140673600027616

22. Nguyen The Tich S, Anderson PJ, Shimony JS, Hunt RW, Doyle LW, Inder TE. A novel quantitative simple brain metric using MR imaging for preterm infants. Am J Neuroradiol. 2009; 30: 125–31. doi: 10.3174/ajnr.A1309 PMID: 18832662

23. Moeskops P, Benders MJNL, Pearlman PC, Kersbergen KJ, Leemans A, Viergever MA, et al. Assessment of quantitative cortical biomarkers in the developing brain of preterm infants. In: Novak CL, Aylward S, editors. SPIE Medical Imaging. 2013. p. 867011. doi: 10.1117/12.2007829

24. Moeskops P, Benders MJNL, Chi ă SM, Kersbergen KJ, Groenendaal F, de Vries LS, et al. Automatic segmentation of MR brain images of preterm infants using supervised classification. Neuroimage. 2015; In press. doi: 10.1016/j.neuroimage.2015.06.007

25. Išgum I, Benders MJNL, Avants B, Cardoso MJ, Counsell SJ, Gomez EF, et al. Evaluation of automatic neonatal brain segmentation algorithms: The NeoBrainS12 challenge. Med Image Anal. 2015; 20: 135–151. doi: 10.1016/j.media.2014.11.001 PMID: 25487610

26. Fischl B, Liu A, Dale A. Automated manifold surgery: constructing geometrically accurate and topologically correct models of the human cerebral cortex. IEEE Trans Med Imaging. 2001; 20: 70–80. Available: http://ieeexplore.ieee.org/xpls/abs_all.jsp?arnumber=906426 PMID: 11293693

27. Windreich G, Kiryati N, Lohmann G. Voxel-based surface area estimation: from theory to practice. Pattern Recognit. 2003; 36: 2531–2541. doi: 10.1016/S0031-3203(03)00173-0

28. Jones SE, Buchbinder BR, Aharon I. Three-dimensional mapping of cortical thickness using Laplace's Equation. Hum Brain Mapp. 2000; 11: 12–32. Available: http://onlinelibrary.wiley.com/doi/10.1002/1097-0193(200009)11:1<12::AID-HBM20>3.0.CO;2-K/full PMID: 10997850

29. Zilles K, Armstrong E, Schleicher A, Kretschmann HJ. The human pattern of gyrification in the cerebral cortex. Anat Embryol. Springer-Verlag; 1988; 179: 173–179. PMID: 3232854

30. Hill J, Dierker D, Neil J, Inder T, Knutsen A, Harwell J, et al. A surface-based analysis of hemispheric asymmetries and folding of cerebral cortex in term-born human infants. J Neurosci. 2010; 30: 2268–76. doi: 10.1523/JNEUROSCI.4682-09.2010 PMID: 20147553

31. Rodriguez-Carranza CE, Mukherjee P, Vigneron D, Barkovich J, Studholme C. A framework for in vivo quantification of regional brain folding in premature neonates. Neuroimage. 2008; 41: 462–478. doi: 10.1016/j.neuroimage.2008.01.008 PMID: 18400518

32. Akaike H. A new look at the statistical model identification. IEEE Trans Automat Contr. 1974; 19. doi: 10.1109/TAC.1974.1100705

33. Dubois J, Benders M, Cachia A, Lazeyras F, Ha-Vinh Leuchter R, Sizonenko SV, et al. Mapping the early cortical folding process in the preterm newborn brain. Cereb Cortex. 2008; 18: 1444–54. doi: 10.1093/cercor/bhm180 PMID: 17934189

34. Pienaar R, Fischl B, Caviness V, Makris N, Grant PE. A methodology for analyzing curvature in the developing brain from preterm to adult. Int J Imaging Syst Technol. 2008; 18: 42–68. doi: 10.1002/ima.20138 PMID: 19936261

35. Awate SP, Yushkevich PA, Song Z, Licht DJ, Gee JC. Cerebral cortical folding analysis with multivariate modeling and testing: Studies on gender differences and neonatal development. Neuroimage. 2010; 53: 450–9. doi: 10.1016/j.neuroimage.2010.06.072 PMID: 20630489

36. Wright R, Kyriakopoulou V, Ledig C, Rutherford MA, Hajnal JV, Rueckert D, et al. Automatic Quantification of Normal Cortical Folding Patterns from Fetal Brain MRI. Neuroimage. 2014; 1–12. doi: 10.1016/j.neuroimage.2014.01.034

37. Li G, Nie J, Wang L, Shi F, Lin W, Gilmore JH, et al. Mapping region-specific longitudinal cortical surface expansion from birth to 2 years of age. Cereb Cortex. 2013; 23: 2724–33. doi: 10.1093/cercor/bhs265 PMID: 22923087

38. Nie J, Li G, Wang L, Gilmore JH, Lin W, Shen D. A computational growth model for measuring dynamic cortical development in the first year of life. Cereb Cortex. 2012; 22: 2272–84. doi: 10.1093/cercor/bhr293 PMID: 22047969

39. Lyall AE, Shi F, Geng X, Woolson S, Li G, Wang L, et al. Dynamic Development of Regional Cortical Thickness and Surface Area in Early Childhood. Cereb Cortex. 2014; 1–9. doi: 10.1093/cercor/bhu027

40. Li G, Wang L, Shi F, Lyall AE, Lin W, Gilmore JH, et al. Mapping longitudinal development of local cortical gyrification in infants from birth to 2 years of age. J Neurosci. 2014; 34: 4228–38. doi: 10.1523/JNEUROSCI.3976-13.2014 PMID: 24647943

41. Hu H-H, Guo W-Y, Chen H-Y, Wang P-S, Hung C-I, Hsieh J-C, et al. Morphological regionalization using fetal magnetic resonance images of normal developing brains. Eur J Neurosci. 2009; 29: 1560–7. doi: 10.1111/j.1460-9568.2009.06707.x PMID: 19419421

42. Clouchoux C, Kudelski D, Gholipour A, Warfield SK, Viseur S, Bouyssi-Kobar M, et al. Quantitative in vivo MRI measurement of cortical development in the fetus. Brain Struct Funct. 2012; 217: 127–39. doi: 10.1007/s00429-011-0325-x PMID: 21562906

43. Kinney HC, Brody BA, Kloman AS, Gilles FH. Sequence of central nervous system myelination in human infancy. II. Patterns of myelination in autopsied infants. J Neuropathol Exp Neurol. 1988; 47: 217–234. PMID: 3367155

44. Huttenlocher PR, Dabholkar AS. Regional differences in synaptogenesis in human cerebral cortex. J Comp Neurol. 1997; 387: 167–78. Available: http://www.ncbi.nlm.nih.gov/pubmed/9336221 PMID: 9336221

45. Volpe JJ. Neurology of the Newborn. 5th ed. Philadelphia: Elsevier; 2008.

46. Kostovic I, Vasung L. Insights from in vitro fetal magnetic resonance imaging of cerebral development. Semin Perinatol. 2009; 33: 220–33. doi: 10.1053/j.semperi.2009.04.003 PMID: 19631083

47. Chugani HT. A critical period of brain development: studies of cerebral glucose utilization with PET. Prev Med. 1998; 27: 184–8. doi: 10.1006/pmed.1998.0274 PMID: 9578992

48. Nossin-Manor R, Card D, Morris D, Noormohamed S, Shroff MM, Whyte HE, et al. Quantitative MRI in the very preterm brain: assessing tissue organization and myelination using magnetization transfer, diffusion tensor and T_1 imaging. Neuroimage. 2013; 64: 505–16. doi: 10.1016/j.neuroimage.2012.08.086 PMID: 22982360

49. De Vis JB, Petersen ET, de Vries LS, Groenendaal F, Kersbergen KJ, Alderliesten T, et al. Regional changes in brain perfusion during brain maturation measured non-invasively with Arterial Spin Labeling MRI in neonates. Eur J Radiol. 2013; 82: 538–43. doi: 10.1016/j.ejrad.2012.10.013 PMID: 23199750

50. Rose J, Vassar R, Cahill-Rowley K, Guzman XS, Stevenson DK, Barnea-Goraly N. Brain microstructural development at near-term age in very-low-birth-weight preterm infants: an atlas-based diffusion imaging study. Neuroimage. 2014; 86: 244–56. doi: 10.1016/j.neuroimage.2013.09.053 PMID: 24091089

51. Deipolyi AR, Mukherjee P, Gill K, Henry RG, Partridge SC, Veeraraghavan S, et al. Comparing microstructural and macrostructural development of the cerebral cortex in premature newborns: diffusion tensor imaging versus cortical gyration. Neuroimage. 2005; 27: 579–86. doi: 10.1016/j.neuroimage.2005.04.027 PMID: 15921934

52. Tzarouchi LC, Astrakas LG, Xydis V, Zikou A, Kosta P, Drougia A, et al. Age-related grey matter changes in preterm infants: an MRI study. Neuroimage. 2009; 47: 1148–53. doi: 10.1016/j.neuroimage.2009.03.072 PMID: 19348950

53. Benders MJ, Palmu K, Menache C, Borradori-Tolsa C, Lazeyras F, Sizonenko S, et al. Early Brain Activity Relates to Subsequent Brain Growth in Premature Infants. Cereb cortex. 2014; 1–11. doi: 10.1093/cercor/bhu097

54. Narberhaus A, Lawrence E, Allin MP, Walshe M, McGuire P, Rifkin L, et al. Neural substrates of visual paired associates in young adults with a history of very preterm birth: alterations in fronto-parieto-occipital networks and caudate nucleus. Neuroimage. 2009; 47: 1884–93. doi: 10.1016/j.neuroimage.2009.04.036 PMID: 19376244

55. Doesburg SM, Chau CM, Cheung TPL, Moiseev A, Ribary U, Herdman AT, et al. Neonatal pain-related stress, functional cortical activity and visual-perceptual abilities in school-age children born at extremely low gestational age. Pain. 2013; 154: 1946–52. doi: 10.1016/j.pain.2013.04.009 PMID: 23711638

56. Chi JG, Dooling EC, Gilles FH. Left-right asymmetries of the temporal speech areas of the human fetus. Arch Neurol. 1977; 34: 346–348. PMID: 860936

57. Kostović I, Judas M. The development of the subplate and thalamocortical connections in the human foetal brain. Acta Paediatr. 2010; 99: 1119–27. doi: 10.1111/j.1651-2227.2010.01811.x PMID: 20367617

58. Lee JD, Park H-J, Park ES, Oh M-K, Park B, Rha D-W, et al. Motor pathway injury in patients with periventricular leucomalacia and spastic diplegia. Brain. 2011; 134: 1199–210. doi: 10.1093/brain/awr021 PMID: 21385750

59. Buser JR, Maire J, Riddle A, Gong X, Nguyen T, Nelson K, et al. Arrested preoligodendrocyte maturation contributes to myelination failure in premature infants. Ann Neurol. 2012; 71: 93–109. doi: 10.1002/ana.22627 PMID: 22275256

60. Back SA, Miller SP. Brain injury in premature neonates: A primary cerebral dysmaturation disorder? Ann Neurol. 2014; 75: 469–86. doi: 10.1002/ana.24132 PMID: 24615937

61. Rakic P. Genetic control of cortical convolutions. Science. 2004; 303: 1983–4. doi: 10.1126/science.1096414 PMID: 15044793

62. Piao X, Hill RS, Bodell A, Chang BS, Basel-Vanagaite L, Straussberg R, et al. G protein-coupled receptor-dependent development of human frontal cortex. Science. 2004; 303: 2033–6. doi: 10.1126/science.1092780 PMID: 15044805

63. Connolly CJ. External morphology of the primate brain. Springfield: CC Thomas; 1950.

64. Richman DP, Stewart RM, Hutchinson JW, Caviness VS. Mechanical Model of Brain Convolutinal Development. Science. 1975; 189: 18–21. PMID: 1135626

65. Welker W. Why does cerebral cortex fissure and fold? A review of determinants of gyri and sulci. In: Jones EG, Peters A, editors. Cerebral cortex. Plenum Press; 1990. pp. 3–136. Available: http://link.springer.com/chapter/10.1007/978-1-4615-3824-0_1

66. Goldman-Rakic PS, Rakic P. Experimental Modification of Gyral Patterns. In: Geschwind N, Galaburda AM, editors. Cerebral Dominance: The Biological Foundations. Cambridge: Harvard University Press; 1984. pp. 179–192.

67. Van Essen D. A tension-based theory of morphogenesis and compact wiring in the central nervous system. Nature. 1997; 385: 313–318. PMID: 9002514

68. Toro R, Burnod Y. A morphogenetic model for the development of cortical convolutions. Cereb Cortex. 2005; 15: 1900–13. doi: 10.1093/cercor/bhi068 PMID: 15758198

69. Hilgetag CC, Barbas H. Developmental mechanics of the primate cerebral cortex. Anat Embryol. 2005; 210: 411–7. doi: 10.1007/s00429-005-0041-5 PMID: 16175385

70. Hilgetag CC, Barbas H. Role of mechanical factors in the morphology of the primate cerebral cortex. PLoS Comput Biol. 2006; 2: e22. doi: 10.1371/journal.pcbi.0020022 PMID: 16557292

71. Neal J, Takahashi M, Silva M, Tiao G, Walsh CA, Sheen VL. Insights into the gyrification of developing ferret brain by magnetic resonance imaging. J Anat. 2007; 210: 66–77. doi: 10.1111/j.1469-7580.2006.00674.x PMID: 17229284

72. Le Provost J-B, Bartres-Faz D, Paillere-Martinot M- L, Artiges E, Pappata S, Recasens C, et al. Paracingulate sulcus morphology in men with early-onset schizophrenia. Br J Psychiatry. 2003; 182: 228–232. doi: 10.1192/bjp.182.3.228 PMID: 12611786

73. Molko N, Cachia A, Rivière D, Mangin J. Functional and structural alterations of the intraparietal sulcus in a developmental dyscalculia of genetic origin. Neuron. 2003; 40: 847–858. Available: http://www.sciencedirect.com/science/article/pii/S0896627303006706 PMID: 14622587

74. Van Essen DC, Dierker D, Snyder AZ, Raichle ME, Reiss AL, Korenberg J. Symmetry of cortical folding abnormalities in Williams syndrome revealed by surface-based analyses. J Neurosci. 2006; 26: 5470–83. doi: 10.1523/JNEUROSCI.4154-05.2006 PMID: 16707799

75. Rees S, Stringer M, Just Y. The vulnerability of the fetal sheep brain to hypoxemia at mid-gestation. Dev brain Res. 1997; 103: 103–118. Available: http://www.sciencedirect.com/science/article/pii/S0165380697817877

76. Dean JM, McClendon E, Hansen K, Azimi-Zonooz A, Chen K, Riddle A, et al. Prenatal cerebral ischemia disrupts MRI-defined cortical microstructure through disturbances in neuronal arborization. Sci Transl Med. 2013; 5: 168ra7. doi: 10.1126/scitranslmed.3004669 PMID: 23325800

77. Ball G, Boardman JP, Rueckert D, Aljabar P, Arichi T, Merchant N, et al. The effect of preterm birth on thalamic and cortical development. Cereb Cortex. 2012; 22: 1016–24. doi: 10.1093/cercor/bhr176 PMID: 21772018

78. Dean JM, Bennet L, Back SA, McClendon E, Riddle A, Gunn AJ. What brakes the preterm brain? An arresting story. Pediatr Res. 2014; 75: 227–33. doi: 10.1038/pr.2013.189 PMID: 24336432

79. Kostović I, Jovanov-Milošević N, Radoš M, Sedmak G, Benjak V, Kostović-Srzentić M, et al. Perinatal and early postnatal reorganization of the subplate and related cellular compartments in the human

cerebral wall as revealed by histological and MRI approaches. Brain Struct Funct. 2014; 219: 231–53. doi: 10.1007/s00429-012-0496-0 PMID: 23250390

80. Xue H, Srinivasan L, Jiang S, Rutherford M, Edwards AD, Rueckert D, et al. Automatic segmentation and reconstruction of the cortex from neonatal MRI. Neuroimage. 2007; 38: 461–77. doi: 10.1016/j. neuroimage.2007.07.030 PMID: 17888685